

Crystal Structure, Vibrational and Electrical Properties of the Bis (phenylammonium) Hexachlorotin(IV): $(C_6H_5NH_3)_2^*SnCl_6$

Sahel Karoui¹, Slaheddine Kamoun²

^{1,2} Laboratory of Materials Engineering and Environment (LR11ES46), BP 1173, ENIS, Sfax University, Tunisia.

Abstract: The X-ray single crystal diffraction has been employed to study the crystal structure of $(C_6H_5NH_3)_2SnCl_6$ at 298K. The crystal structure is monoclinic, space group $P2_1/c$, $Z=4$, $a=7.116(5)\text{\AA}$, $b=25.304(2)\text{\AA}$, $c=11.686(9)\text{\AA}$ and $\beta=90.239(4)^\circ$. The structure was solved from 4041 independent reflections with $R_1=0.0328$ and $wR_2=0.0822$ and refined with 212 parameters. The crystal is built up of separated $(SnCl_6)^{2-}$ octahedral anions and two phenylammonium cations. These chains are themselves interconnected by means of N-H...Cl hydrogen bonds originating from the organic cation $(C_6H_5NH_3)^+$. The Infrared and Raman spectra of this compound have been recorded at room temperature and discussed in relation to the crystal structure of a made-up $(C_6H_5NH_3)_2SnCl_6$ sample. The alternative current (ac) conductivity of the compound $(C_6H_5NH_3)_2SnCl_6$ has been measured in the temperature range 314–368 K and the frequency range 209 Hz–5MHz. The Cole-Cole (the imaginary part (Z'') versus real part (Z') of impedance complex) plots are well fitted to an equivalent circuit model which consists of a parallel combination of a bulk resistance (R_p) and constant phase elements (CPE). The single semicircle indicates only one primary mechanism for the electrical conduction with in $(C_6H_5NH_3)_2SnCl_6$.

Keywords: Organic-inorganic hybrid; Crystal structure; Powder diffraction; IR spectroscopy; RAMAN spectroscopy; Dielectric properties.

1. Introduction

Recently, the researches on inorganic-organic hybrid compounds have been advanced in the field of material science [1]. At the molecular level, the combination of two extremely different components provides a way to design new hybrid materials as well as the ability to modulate properties of one or more components [2, 3]. Some attractive properties, such as ideal thermal and mechanical stability, interesting magnetic [4], non-linear optical [3] etc, which the individual inorganic or organic components do not have, can be observed in hybrid materials. A typical research focused on the low-dimensional inorganic-organic hybrid materials formulated as $R_xM_yX_z$ (where R is the protonated amine; M = metal; X = halide anion), which are characterized by corner-sharing $[MX_6]$ octahedral [5, 6] separated by protonated amine cations. In contrast, little attention has been paid to the isolated compounds [7, 8].

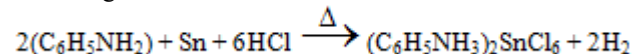
We report herein the synthesis, crystal structure, DSC, X-rays powder diffraction, the vibrational spectroscopy (Infrared (IR) and Raman) and the impedance spectroscopic analysis of a new organic Sn(IV) hexachloro complex: $(C_6H_5NH_3)_2SnCl_6$. The impedance spectroscopy measurements were analyzed using various formalisms, such as the complex impedance $Z^* = Z'(\omega) - jZ''(\omega)$ and the complex conductivity $\sigma^* = \sigma'(\omega) + j\sigma''(\omega)$.

2. Experimental Section

2.1. Chemical Preparation

$(C_6H_5NH_3)_2SnCl_6$ was prepared by refluxing a solution of metallic tin (3g, 25 mmol) during 5 h in a 40 ml aqueous solution of HCl (2M). For this propose, 9.5 ml (75 mmol) of

a solution of phenylamine at reflux temperature was added. After a slow solvent evaporation, yellow crystals suitable for X-ray analysis were obtained. They were filtered and washed with diethyl ether and dried over P_2O_5 . The reactions sequence for the synthesis may be described by the following chemical reaction:



2.2. Investigation Techniques

The title compound was studied through various physico-chemical methods such as, the X-ray diffraction, thermal analysis, the X-ray powder diffraction, Raman, IR and Impedance spectroscopy.

2.2.1. X-ray Diffraction

A suitable colorless crystal, which was selected under a polarizing microscope and mounted on a glass fiber, was chosen for the structure determination. The Experimental conditions used for the single-crystal diffraction data collection and structure refinement are reported in Table 1. The positional parameters for the stannate and the chloride atoms were obtained from the three-dimensional Patterson map, whereas the remaining atoms were acquired from successive difference Fourier maps. After introducing anisotropic thermal factors for the non-hydrogen atoms and isotropic thermal factors for H atoms, the hydrogen atoms

Table 1: Crystal and refinement data of $(C_6H_5NH_3)_2SnCl_6$

Formula	$(C_6H_5NH_3)_2SnCl_6$
Molecular weight (g.mol ⁻¹)	519.68
Crystal System	Monoclinic
Temp (K)	293(2)
Space group	P2 ₁ /c
a, (Å)	7.1166 (5)
b, (Å)	25.304(2)
c, (Å)	11.6862(9)
β (°)	90.239(4)
V (Å ³)	2104.4 (3)
Z	4
Dcalc. (g.cm ⁻³)	1.640
F (000)	1016
μ (mm ⁻¹)	1.970
Crystal size (mm)	0.4 x 0,16 x 0,07
Color, shape	Colourless / parallélépipède
θ_{min} , θ_{max} (deg)	3.285- 28.256
No. of reflections collected	5075
No. of independent reflections $I > 2\sigma(I)$	4041
No. of parameters	212
R_1^a , wR_2^b	$R_1 = 0.0328$, $wR_2 = 0.0822$
Goodness-of fit on F^2	1.034
Deposit number (CCDC)	CCDC 924479
$R_1^a = \frac{\sum F_o - F_c }{\sum F_o }$	$wR_2^b = \frac{\sqrt{\sum (F_o - F_c)^2}}{\sqrt{\sum F_o ^2}}$

were localized and optimized to fixed positions. Although their contribution was isotropically introduced into calculation, these hydrogen atoms were not refined. Corrections were applied for Lorentz and polarization effects and absorption. The final refinement cycles with 2502 reflections correspond to $I > 2\sigma(I)$ yielded $R = 0.034$ and $R_w = 0.094$. All calculations were performed using SHELXS and SHELXL included in the WINGX package [9].

2.2.2. Thermal Behaviour

Differential scanning calorimetry (DSC) measurements were performed by heating 10 mg of the sample from 270 K to 480 K on a Perkin Elmer apparatus (Model 4000), at a heating rate of 5 Kmin⁻¹.

2.2.3. Powder Diffraction Analysis

X-ray powder diffraction data were collected at a temperature range of 285K to 325 K using a SIEMENS D500 powder diffractometer with $CuK\alpha_1$ radiation, in the $2-\theta$ range from 5.00° to 60.00° with a step length of 0.02°.

2.2.4. Raman and IR Spectroscopy

Raman spectra of the sample was recorded at room temperature using 633 nm line laser as excitation wave length in the region 200–4000 cm⁻¹ on a LabRAM HR 800 set up. The incident power was kept less than 40 mW to avoid the degradation of the sample by heating. The infrared spectrum was recorded at room temperature, in 400–4000 cm⁻¹ spectral range with a 4 cm⁻¹ resolution, by using a Perkin-Elmer FT IR spectrometer (spectrum one model). The $(C_6H_5NH_3)_2SnCl_6$ salts were ground in a clean mortar

into fine powder and a small quantity of it was mixed and ground with KBr in order to make a 1mm thickness pellet by using a 2 t press.

2.2.5. Impedance Spectroscopy

The $(C_6H_5NH_3)_2SnCl_6$ polycrystalline sample was pressed at room temperature under 15 MPa. A pellet of about 8 mm in diameter and 2 mm in thickness was used for the electrical measurements. The dielectric properties were measured using an TEGAM 3550 ALF precision Impedance Analyzer, in the C_p-R_p configuration. The temperature was controlled with accuracy up to 0.1 K. The measurements were performed at the temperature range of 314–368 K, in the frequency range of 200 Hz–5MHz. The iterative nonlinear least-squares fitting were made using Microcal Origin 6.0 software. The values of R (regression coefficient indicating goodness of fit) for all the fittings are greater than 0.9989.

3. Results and discussion

3.1. Crystal Structure Description

The asymmetric unit of the title compound $(C_6H_5NH_3)_2SnCl_6$ consists of two phenylammonium cations and one independent octahedral $(SnCl_6)^{2-}$ anion Fig. 1. The crystal structure which consists in alternating organic and inorganic layers extending parallel to the ab plane is illustrated in Fig. 2. The organic layer contains the aromatic rings, whereas the

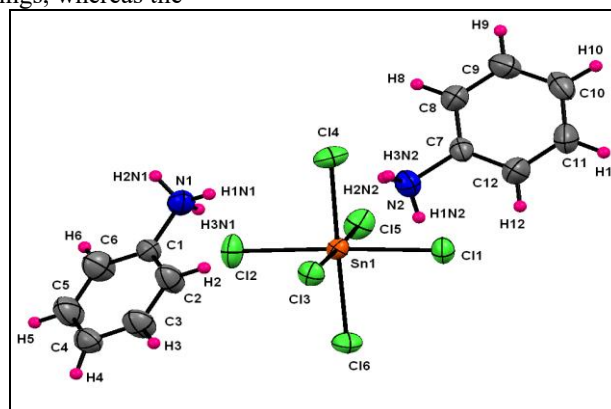


Figure 1: A view of the asymmetric unit of the title compound

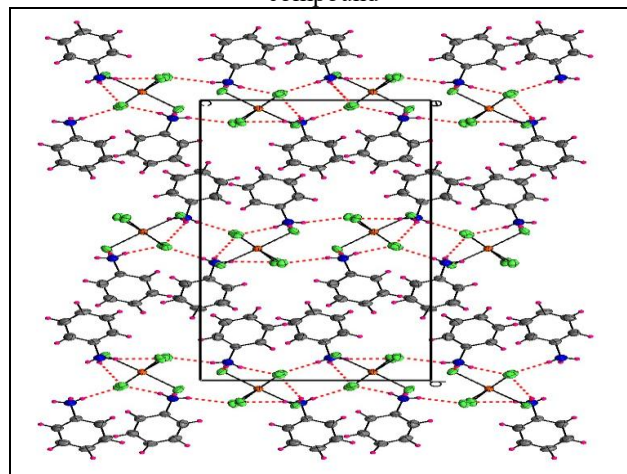


Figure 2: Projection along the c-axis of the atomic arrangement of $(C_6H_5NH_3)_2SnCl_6$

inorganic layer comprises the ammonium groups and independent $(\text{SnCl}_6)^{2-}$ octahedra. In order to study the influence of cations on crystal structures of organic ammonium hexachlorostannate (IV) hybrids, several crystals of this type were prepared and their structures were determined [10, 11]. The general structure displays an alternation of the hydrocarbon layers made up of ammonium cations, and inorganic layers made up of discrete SnCl_6 octahedra. The interface between the inorganic and organic layers contains Cl^- and $-\text{NH}_3^+$ ions in which charge-assisted hydrogen bonds connect two kinds of layers. The asymmetric unit of the title crystal structure consists of two phenylammonium cations on general positions. The Sn atom is six-coordinated and forms a quasi-regular octahedral arrangement [23]. This $(\text{SnCl}_6)^{2-}$ octahedron alternates with the cationic layers along the c axis Fig. 2. The bond lengths are similar to those found in other octahedral Sn(IV) compounds [12]. The Sn(1)—Cl bond lengths are 2.400(1), 2.442(1), and 2.446(1) Å, the cis Cl—Sn(1)—Cl bond angles range from 89.04(4)° to 90.96(4)°, indicating small distortions from ideal octahedral geometry, Table 2. A similar configuration of the $(\text{SnCl}_6)^{2-}$ anion was also found for $(\text{HPPPh}_3)_2\text{SnCl}_6$ [13] and $(\text{C}_7\text{H}_{10}\text{NO})\text{SnCl}_3$ [14]. The average values of the distortion parameters of SnCl_6 octahedra are calculated using the following equations (1)–(5) [15].

Table 2: Principal intermolecular distances (Å) and bond angles (°) in $(\text{SnCl}_6)^{2-}$ anion.

Sn(1)-Cl(1)	2.4173 (8)	Sn(1)-Cl(4)	2.4217 (8)
Sn(1)-Cl(2)	2.4282 (8)	Sn(1)-Cl(5)	2.4158 (8)
Sn(1)-Cl(3)	2.4369 (7)	Sn(1)-Cl(6)	2.4510 (8)
Cl(1)-Sn(1)-Cl(2)	177.61(3)	Cl(2)-Sn(1)-Cl(6)	90.00(3)
Cl(1)-Sn(1)-Cl(3)	90.75(3)	Cl(3)-Sn(1)-Cl(4)	87.91(3)
Cl(1)-Sn(1)-Cl(4)	90.76(3)	Cl(3)-Sn(1)-Cl(5)	177.34(3)
Cl(1)-Sn(1)-Cl(5)	91.90(3)	Cl(3)-Sn(1)-Cl(6)	89.72(3)
Cl(1)-Sn(1)-Cl(6)	87.65(3)	Cl(4)-Sn(1)-Cl(5)	92.04(3)
Cl(2)-Sn(1)-Cl(3)	88.77(3)	Cl(4)-Sn(1)-Cl(6)	177.13(3)
Cl(2)-Sn(1)-Cl(4)	91.57(3)	Cl(5)-Sn(1)-Cl(6)	90.39(3)
Cl(2)-Sn(1)-Cl(5)	88.58(3)		

$$\Delta_{\text{oct}} = \frac{1}{6} \sum_{j=1}^6 \left[\frac{(d_j - d_m)}{d_m} \right]^2 \quad (1)$$

$$\sigma_{\text{oct}} = \frac{1}{11} \sum_{j=1}^{12} [(\alpha_j - 90)]^2 \quad (2)$$

$$\text{ID}_{(\text{Sn-X})} = \frac{\left(\sum_{i=1}^6 |d_i - d_m| \right)}{6d_m} \quad (3)$$

$$\text{ID}_{(\text{X-Sn-X})} = \frac{\left(\sum_{i=1}^{12} |\alpha_i - \alpha_m| \right)}{12\alpha_m} \quad (4)$$

$$\text{ID}_{(\text{X-X})} = \frac{\left(\sum_{i=1}^{12} |(X-X)_i - (X-X)_m| \right)}{12(X-X)_m} \quad (5)$$

With α_i : (Cl-Sn-Cl) angle, d: (Sn-Cl) distance, X: (Cl-Cl) distance, m: average values. $\Delta_{\text{oct}}=0.012$, $\sigma_{\text{oct}}^2=31.164$, $\text{ID}(\text{Sn-Cl})=0.101$, $\text{ID}(\text{Cl-Sn-Cl})=0.042$ and $\text{ID}(\text{Cl-Cl})=$

0.121. The low values of the distortion indices indicate that the coordination geometry of the metal is a slightly distorted octahedral; this can be explained by the stereochemical inactivity of the $5s^2$ lone pair of Sn (IV). The cations pack in an interdigitated fashion within the organic layers, whose thickness is about two phenylammonium lengths along the long molecular axis. The C—C bond lengths in the phenyl ring range from 1.328(8) Å to 1.389(9) Å with the mean value of 1.365(8) Å, while mean C—N bond lengths are 1.466(5) Å. C—C—C angles in phenyl ring are between 118.5(4)° and 121.8(4)° Table 3. The hydrogen bonding interactions linking the organic and the inorganic layer involve the

Table 3: Principal intermolecular distances (Å) and bond angles (°) in $(\text{C}_6\text{H}_5\text{NH}_3)^+$.

C(1)-C(2)	1.373(4)	C(7)-C(8)	1.357(5)
C(2)-C(3)	1.389(5)	C(8)-C(9)	1.379(5)
C(3)-C(4)	1.377(5)	C(9)-C(10)	1.382(6)
C(4)-C(5)	1.375(5)	C(10)-C(11)	1.373(6)
C(5)-C(6)	1.393(5)	C(11)-C(12)	1.388(5)
C(1)-C(6)	1.365(5)	C(7)-C(12)	1.360(5)
C(1)-N(1)	1.480(4)	C(7)-N(2)	1.474(4)
C(2)-H(2C2)	0.93	C(8)-H(8C8)	0.93
C(3)-H(3C3)	0.93	C(9)-H(9C9)	0.93
C(4)-H(4C4)	0.93	C(10)-H(10C10)	0.93
C(5)-H(5C5)	0.93	C(11)-H(11C11)	0.93
C(6)-H(6C6)	0.93	C(12)-H(12C12)	0.93
N(1)-H(1N1)	0.89	N(2)-H(1N2)	0.89
N(1)-H(2N1)	0.89	N(2)-H(2N2)	0.89
N(1)-H(3N1)	0.89	N(2)-H(2N2)	0.89
C(1)-C(2)-C(3)	119.2(3)	H(1N1)-N(1)-H(2N1)	109.5
C(2)-C(3)-C(4)	121.6(4)	H(1N1)-N(1)-H(3N1)	109.5
C(3)-C(4)-C(5)	117.5(4)	H(2N1)-N(1)-H(3N1)	109.5
C(4)-C(5)-C(6)	122.0(4)	C(1)-C(2)-H(2)	120.4
C(5)-C(6)-C(1)	118.8(4)	C(2)-C(3)-H(3)	119.2
C(6)-C(1)-C(2)	120.8(3)	C(4)-C(3)-H(3)	119.2
C(6)-C(1)-N(1)	119.1(3)	C(3)-C(2)-H(2)	120.4
C(2)-C(1)-N(1)	120.0(3)	C(7)-C(8)-H(8)	120.4
C(7)-C(8)-C(9)	119.2(3)	C(9)-C(8)-H(8)	120.4
C(8)-C(9)-C(10)	121.3(4)	C(8)-C(9)-H(9)	119.3
C(9)-C(10)-C(11)	117.7(4)	C(10)-C(9)-H(9)	119.3
C(10)-C(11)-C(12)	121.4(4)	C(11)-C(10)-H(10)	116
C(8)-C(7)-C(12)	121.4(3)	C(9)-C(10)-H(10)	126
C(7)-C(12)-C(11)	118.9(4)	C(10)-C(11)-H(11)	119.3
C(8)-C(7)-N(2)	119.2(3)	C(12)-C(11)-H(11)	119.3
C(12)-C(7)-N(2)	119.4(3)	C(7)-C(12)-H(12)	120.5
C(1)-C(6)-H(6)	120.6	C(11)-C(12)-H(12)	120.5
C(4)-C(5)-H(5)	119	C(7)-N(2)-H(1N2)	109.5
C(5)-C(6)-H(6)	120.6	C(7)-N(2)-H(2N2)	109.5
C(6)-C(5)-H(5)	119	C(7)-N(2)-H(3N2)	109.5
C(1)-N(1)-H(1N1)	109.5	H(1N2)-N(2)-H(2N2)	109.5
C(1)-N(1)-H(2N1)	109.5	H(1N2)-N(2)-H(3N2)	109.5
C(1)-N(1)-H(3N1)	109.5	H(2N2)-N(2)-H(3N2)	109.5

Table 4: Hydrogen-bond geometry (Å, °)

D—H...A	D—H	H...A	D...A	D—H...A
N(1)-(H1N1)...Cl(6) ⁽ⁱ⁾	0.89	2.51	3.387(3)	167
N(1)-(H2N1)...Cl(5) ⁽ⁱⁱ⁾	0.89	2.55	3.416(3)	164
N(1)-(H3N1)...Cl(2)	0.89	2.59	3.456(3)	165
N(2)-(H1N2)...Cl(3) ⁽ⁱⁱⁱ⁾	0.89	2.46	3.351(3)	174
N(2)-(H2N2)...Cl(4)	0.89	2.53	3.411(3)	172
N(2)-(H3N2)...Cl(6) ⁽ⁱ⁾	0.89	2.64	3.326(3)	134

(i) -1+x, y, z; (ii) 1-x, 1-y, 1-z; (iii) 1-x, 1-y, -z.

two hydrogen atoms on the ammonium group. There are one-simple and one-bifurcated hydrogen bonds between a cation and three different Cl atoms Fig. 2. Atoms N1 and N2 of the phenylammonium participate in the formation of strong inter- and intra-molecular (N—H...Cl) hydrogen bonds with hexachlorostannate and phenylammonium (Table 4).

3.2. Differential Scanning Calorimetry (DSC)

The differential scanning calorimetry was performed on heating a $(C_6H_5NH_3)_2SnCl_6$ sample from 290 to 430K. The thermal analysis results are reported in Fig. 3. The thermogram shows two endothermic peaks at $T_1=343$ K and $T_2=395$ K. The enthalpy and entropy values for these transitions are respectively $\Delta H_1=8.79$ kJ mol⁻¹ and $\Delta S_1=25.626$ J mol⁻¹ K⁻¹ for the former and $\Delta H_2=161.578$ kJ mol⁻¹ and $\Delta S_2=0.409$ kJmol⁻¹ K⁻¹ for the latter, which corresponds to the melting point. Where ΔH represents the calorimetric enthalpy, which represents the total integrated zone below the thermogram peak, indicating the total heat energy uptake by the sample after suitable baseline correction. It is calculated as follows:

$$\int \left(\frac{dH}{dT} \right)_{Sample} dt = \Delta H_{Sample} \quad (6)$$

and $\Delta S = \frac{\Delta H}{T}$, the entropy change per mole of the sample, where T is the absolute temperature.

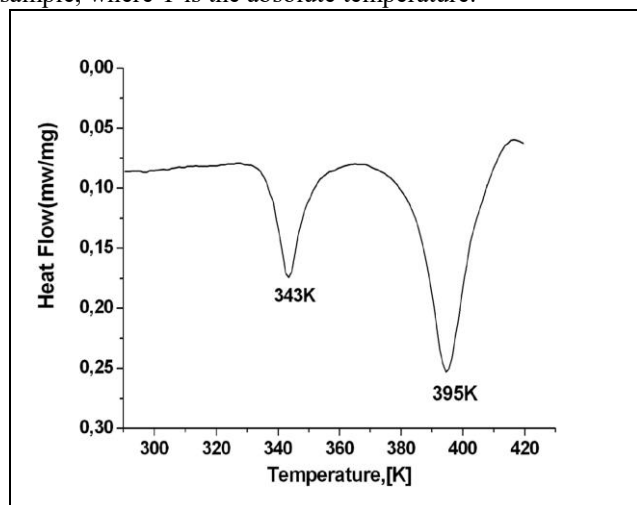


Figure 3: Differential scanning calorimeter run on $(C_6H_5NH_3)_2SnCl_6$

3.3. Powder Diffraction Analysis

In order to get more information about the mechanism of phase transition, we have studied the evolution of the X-ray powder diffraction at a temperature range from 298 K to 368

K. Fig. 4 shows the successive powder patterns obtained through heating.

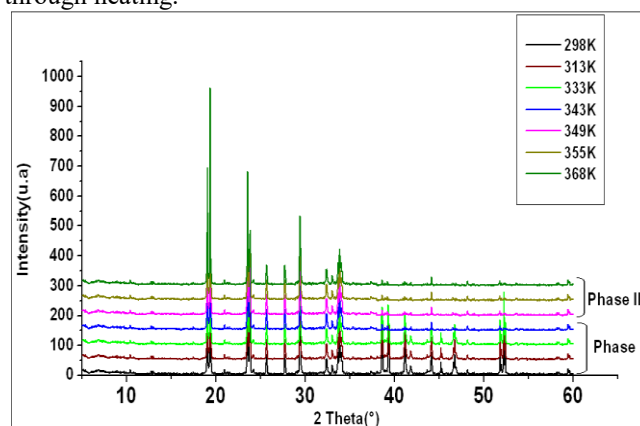


Figure 4: Temperature dependence of the X-ray diffraction patterns of $(C_6H_5NH_3)_2SnCl_6$

The lines of the powder pattern of $(C_6H_5NH_3)_2SnCl_6$ were indexed using the dichotomy-method program DICVOL04 [16], on the basis of a monoclinic solution. At 368 K, $(C_6H_5NH_3)_2SnCl_6$ crystallizes in the monoclinic system Pm with the following lattice parameters, $a=9,234(5)$, $b=22,124(2)$, $c=6,786(9)$ Å, and $\beta=98,754(4)^\circ$ and with a figure of merit of $F_{50}(0.0543, 76)=28$. The temperature dependencies of the lattice parameters a , b , c , β and the volume of the unit cell over the temperature range, 298–368K, are shown in Fig. 5. One anomaly of the lattice parameters is observed close to 368 K, which corresponds to the structural phase transition disclosed by DSC measurements. The volume of the unit cell can be well approximated over the wide temperature region by a straight line, except for the vicinity of the I→II transition phase.

4. Vibrational Study

4.1. Group Theoretical Analysis

Phenylammonium $C_6H_5NH_3^+$ contains 15 atoms giving rise to 39 internal vibrational modes. For the assumed Cs symmetry point group of the cation, these internal modes are classified as: $26A'(IR, R) + 13A''(IR, R)$. The phenylammonium cation consists of the benzene, which is linked to NH_3 group and thus has been considered as monosubstituted benzene. Of these 39 internal vibrations, 30 modes belong to the benzene ring and the 9 remaining ones may be assigned to the NH_3 group. In the case of this monosubstituted benzene, all vibrational modes are both infrared and Raman active. The internal vibrational modes of the free $SnCl_6^{2-}$ anion in an assumed O_h symmetry are

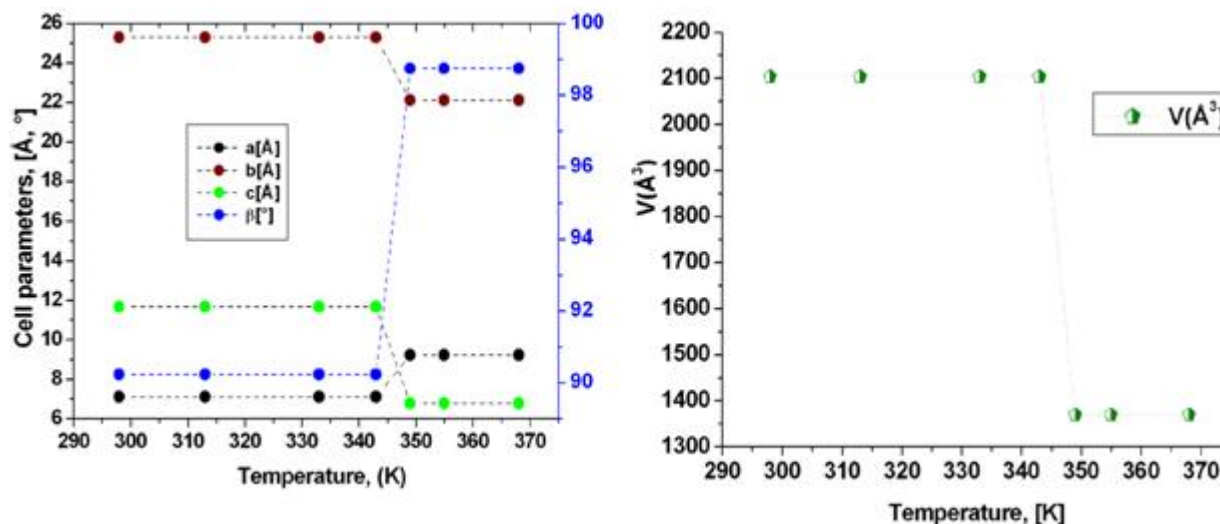


Figure 5: Temperature dependence of cell parameters and volume of the monoclinic system of $(C_6H_5NH_3)_2SnCl_6$

classified as: $1A_{1g}$ (Ra) + $1E_g$ (Ra) + $1F_{2g}$ (Ra) + $2F_{1u}$ (IR) + $1F_{2u}$ (IR). As indicated for the isolated ions, all the cationic vibrational modes are infrared and Raman active; whereas for the anionic ones, only the F_{1u} and F_{2u} modes are infrared active while the modes of A_{1g} , E_g and F_{2g} type are Raman observable.

4.2. Infrared and Raman spectrum of $(C_6H_5NH_3)_2SnCl_6$

The Infrared and Raman spectrum of the $(C_6H_5NH_3)_2SnCl_6$ compounds are shown in Figs. 6 and 7. The factor group analysis for cation and anion modes in this crystal is given in Tables 5 and 6, respectively. The wavenumbers of the observed IR and Raman bands are listed in Table 7. The assignment of these bands was made by comparison with previous works done on analogous compounds.

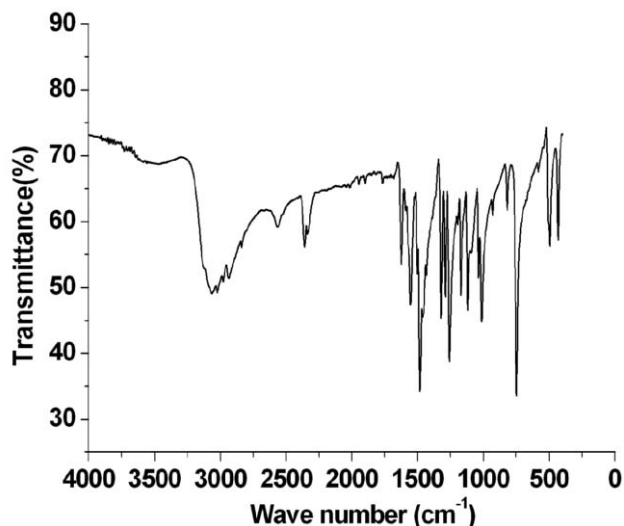


Figure 6: IR ambient temperature spectrum of $(C_6H_5NH_3)_2SnCl_6$

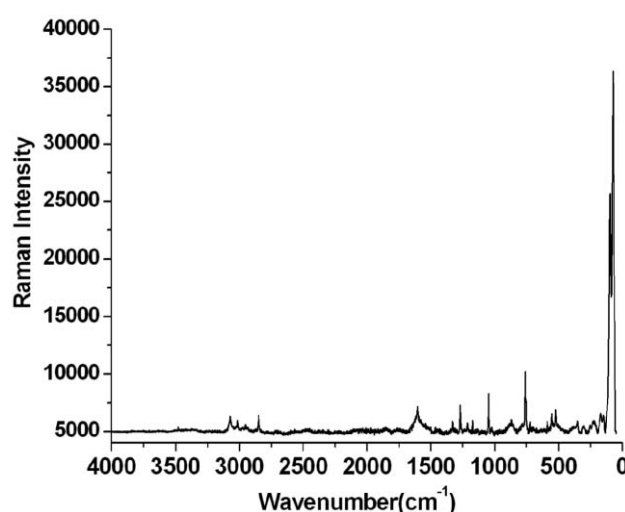


Figure 7: Raman ambient temperature spectrum of $(C_6H_5NH_3)_2SnCl_6$

4.3. Phenylammonium internal optics modes

In the infrared spectra of partially substituted benzene, one band is observed between 3100 and 3000 cm^{-1} , and two or three may occur. At room temperature, the infrared and Raman spectrum of $(C_6H_5NH_3)_2SnCl_6$ exhibit in this range one strong and very broad feature having a width of 300–350 cm^{-1} [17] in its halfhigher. This band may be due to $\nu_{(CH)}$ stretching modes of aromatic ring and some $\nu_{S(NH_3)}$ symmetric stretching of NH_3 group. The broadening of this infrared band may be explained by its overlapping CH aromatic and NH stretching modes therefore it is an indicative of the formation of strong hydrogen bonding of type N-H...Cl that linked $SnCl_6^{2-}$ anions and $C_6H_5NH_3^+$ cations inside the crystal. At room temperature, the Raman spectrum of this compound exhibited, in this range, one intense band at 3073 cm^{-1} which was assigned to $\nu_{(CH)}$ stretching modes of the benzene ring. It has been observed that benzene derivatives possess overtone or combination tone vibrations that give rise to infrared absorption between 2000 and 1700 cm^{-1} [18, 19]. In the infrared spectrum of this compound, most of the bands in the region 2000 and 2800 cm^{-1} may also be due to the non-fundamental bands of the benzene ring. An attempt of the assignment of these non-

fundamental bands leads us to propose them as combinations and overtone vibrations as given in Table 7.

In the infrared spectra of substituted benzene, bands are commonly observed between 1400 and 1450, and between 1600 and 1550 cm^{-1} in the simpler derivatives [20]. In the monosubstituted benzene such as the phenylammonium cation, there was a removal degeneracy of the benzene degenerate modes, which implies that all their vibrational modes seem to be simultaneously infrared and Raman active. Thus, the $(\text{C}_6\text{H}_5\text{NH}_3)_2\text{SnCl}_6$ infrared spectrum at room temperature shows, in this region several, strong bands

(1470, 1500, 1540 and 1580 cm^{-1}) in which some shoulders take place as has been seen for the very strong feature at 1470 cm^{-1} . Other weak bands were observed in this spectral region near 1370–1390 and 1610–1620 cm^{-1} . In the Raman spectrum, one medium band observed at 1612 cm^{-1} was due to the $\nu_{(\text{C}-\text{C})}$ stretching modes of the benzene ring. We would notice that asymmetric and symmetric stretching vibrational modes of NH_3 group participate to give rise to such features in this region and this may also explain the multiplicity of bands appeared in 1640–1370 cm^{-1} of the infrared spectrum of $(\text{C}_6\text{H}_5\text{NH}_3)_2\text{SnCl}_6$.

Table 5: Correlation diagram for the $(\text{C}_6\text{H}_5\text{NH}_3)^+$ cations

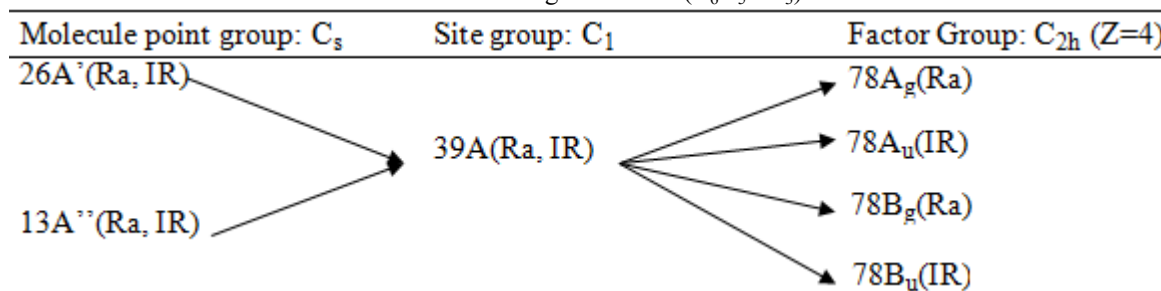
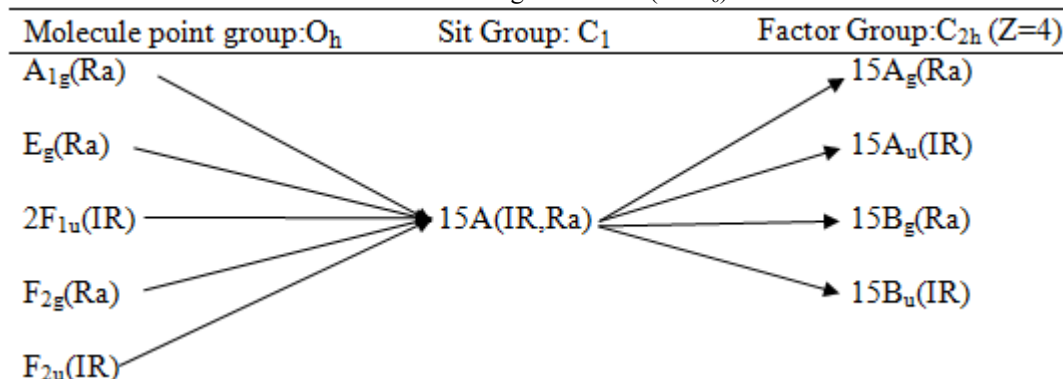


Table 6: Correlation diagram for the $(\text{SnCl}_6)^{2-}$ anions



The Bands corresponding to in-plane vibrational modes of benzene ring generally appear in 1300–1000 cm^{-1} [21, 22]. In the case of the infrared spectrum of $(\text{C}_6\text{H}_5\text{NH}_3)_2\text{SnCl}_6$, we observe several weak, medium and strong bands relative to the in-plane $\delta_{(\text{CH})}$ vibrational modes as has been illustrated in Table 7. The corresponding Raman in-plane $\delta_{(\text{CH})}$ vibrations give rise to several features between 1040 and 1216 cm^{-1} as has been given in Table 7. The multiplicity of the bands appearing in this region can be explained by such splitting of some infrared degenerate modes corresponding to the free benzene ring as well as by the eventual activation of some Raman bands under the lowering of symmetry effect when the benzene ring is monosubstituted. Bands corresponding to these modes have been studied extensively in the simple substituted benzene [23, 24]. The infrared spectrum of $(\text{C}_6\text{H}_5\text{NH}_3)_2\text{SnCl}_6$ shows several bands corresponding to the out-of-plane vibrational modes $\delta_{(\text{CH})}$ in the 950–650 cm^{-1} spectral range; for example, these modes give rise to one strong band at 700 cm^{-1} and some other weak features near 870 and 910 cm^{-1} . The corresponding Raman out-of-plane $\delta_{(\text{CH})}$ modes were observable at 798 (s), 813 and 830 cm^{-1} . The medium infrared band at 992 cm^{-1} which is accompanied by two other weak bands near 1000 cm^{-1} may be due to the vibrational Raman “breathing mode” of the benzene ring becoming active in the infrared spectrum. The

Raman breathing mode has been observed at 1006 in the Raman spectrum. There is also a breathing mode named “trigonal breathing mode” when the benzene is monosubstituted which may be the origin of the two infrared features at 1000 and 1010 cm^{-1} . The specificity and the nature of some infrared absorption of the substituted benzene ring below 650 cm^{-1} have been discussed [25, 26]. In this region of the infrared spectrum of $(\text{C}_6\text{H}_5\text{NH}_3)_2\text{SnCl}_6$, different bands were observed and can be assigned to the out-of-plane $\delta_{(\text{C}-\text{C})}$ vibrational modes, especially the medium bands appeared at 620 and 520 cm^{-1} . The remaining weak bands observed between 520 and 240 cm^{-1} originated from motions of the benzene ring and aromatic C–H bonds. Below 650 cm^{-1} of the Raman spectrum, two bands were observed at 619 and 519 cm^{-1} and were assigned to the out-of-plane $\delta_{(\text{C}-\text{C})}$ modes.

4.4. Internal vibrational modes of SnCl_6^{2-}

The free SnCl_6^{2-} ion strictly assumes the O_h symmetry and has 15 vibration degrees of freedom and the modes, which are possible assuming this symmetry, are summarized as: $\Gamma = 1A_{1g}(\text{Ra}) + 1E_g(\text{Ra}) + 1F_{2g}(\text{Ra}) + 2F_{1u}(\text{IR}) + 1F_{2u}(\text{IR})$. In this crystal of $\text{P2}_1/\text{c}$ space group, the anions are expected to occupy crystal sites of symmetry lower than O_h . As a

result of the four formula units per primitive unit cell, each of the A_{1g} , E_g , F_{1u} , F_{2u} and

Table 7: Assignment of Raman and infrared spectra of $(C_6H_5NH_3)_2SnCl_6$ at room Temperature

Assignment	IR	Raman	Assignment	IR	Raman
$\nu_s(C-H)$	240 vw	-	$\delta(CH)$	1040 s	1040 m
$\nu_s(C-H)$	265 w	-	$\delta(CH)$	1050 w	-
$\nu_s(C-H)$	310 vw	-	$\delta(CH)$	1100 m	-
$\nu_s(C-H)$	330 vw	-	$\delta(CH)$	1120 s	-
$\nu_s(C-H)$	350 vw	-	$\delta(CH)$	1140 w	-
$\delta_{as}(Cl-Sn-Cl)$	390 m	410 w	$\delta(CH)$	-	1164 vw
$\delta_{as}(Cl-Sn-Cl)$	460 vs	-	$\delta(CH)$	1180 vw	1180 m
$\delta(CC)$	520 m	519 w	$\delta(CH)$	1200 vw	-
$\delta(CC)$	620 m	619 m	$\delta(CH)$	1215 vs	1216 m
$\nu_s(Sn-Cl)$	-	650 m	$\delta(CH)$	1300 s	-
$\delta(CH)$	700 s	-	$\delta(CH)$	1320 m	-
$\nu_s(Sn-Cl)$	710 vs	-	$\nu(C-C)$	1370 m	-
$\delta(CH)$	-	798 s	$\nu(C-C)$	1390 vw	-
$\delta(CH)$	-	815 w	$\nu(C-C)$	1470 vw	-
$\delta(CH)$	870 vw	-	$\nu(C-C) + \delta_s(NH_3)$	1500 vw	-
$\delta(CH)$	910 vw	-	$\nu(C-C) + \delta_s(NH_3) + \nu(C-N)$	1540 s	-
$\delta(CH)$	992 m	-	$\nu(C-C) + \nu_{as}(NH_3)$	1580 s	-
$\delta(CH)$	1000 w	-	$\nu(C-C) + \delta_{as}(NH_3)$	1610 w	1612 m
$\delta(CH)$	1010 vw	1006 vs	$\nu(C-H) + \nu_s(NH_3)$	2800 vs,b	3073 m
$\delta(CH)$	1040 s	1040 m	$\nu_{as}(NH_3)$	3435 m,b	-

vs: very strong, s: strong, w: weak, m: medium, vw: very weak, b: broad, s: symmetric, as: asymmetric F_{2g} should split into four components among which only two are Raman-active. The frequencies of $SnCl_6^{2-}$ modes in $(C_6H_5NH_3)_2SnCl_6$ are summarized in Table 7. By comparison with previous works reported on similar compounds containing $[SnCl_6^{2-}]$ [27, 28], the strong band at 710 cm^{-1} was assigned to the $\nu_{as}(Sn-Cl)$ asymmetric

$$Z' = \frac{R_p [1 + R_p Q \omega^\alpha \cos(\frac{\alpha\pi}{2})]}{(1 + R_p Q \omega^\alpha \cos(\frac{\alpha\pi}{2}))^2 + (R_p Q \omega^\alpha \sin(\frac{\alpha\pi}{2}))^2} \quad (8)$$

The iterative nonlinear least-squares fit between the experimental and the theoretical values of the equivalent circuit parameters are illustrated in Figs. 8 and 9 (red line). These results demonstrate the adequacy of the proposed equivalent circuit for the chosen range temperature (314K-

stretching mode, while the very strong feature at 460 cm^{-1} corresponds to the $\delta_{as}(Cl-Sn-Cl)$ asymmetric bending mode. The band of medium intensity at 390 cm^{-1} may be considered as a Raman anionic mode $\delta_s(Cl-Sn-Cl)$, theoretically non-IR active, but becoming infrared observable by the site-field effect lowering the symmetry of $SnCl_6^{2-}$ anion in the $(C_6H_5NH_3)_2SnCl_6$ crystal. In the Raman spectrum, the $SnCl_6^{2-}$ anion internal modes were observed as a medium band at 650 cm^{-1} and a weak one at 410 cm^{-1} . These modes correspond to the $\nu_s(Sn-Cl)$ symmetric stretching mode and to the $\delta_{as}(Cl-Sn-Cl)$ deformation mode, respectively [27].

5. Impedance Analysis

5.1. Cole-Cole plot

The variation of the real (Z') and imaginary (Z'') parts of impedance with frequency at various temperatures is illustrated in Fig. 8. The frequency dependences of Z' and Z'' at several temperatures are shown in Figs. 8a and b. As can be seen, when the temperature increases, Z' arcs move to lower values, indicating an increase in AC conductivity. All the semicircles exhibit some compression instead of a semicircle centered on the x-axis. Such behavior indicates a non-Debye type of relaxation in $(N(C_3H_7)_4)_2SnCl_6$ [29]. For the plots of Figs. 8 and 9, the equivalent circuit of the crystal under AC electric field can be modeled as a resistor R_p in parallel with a constant phase element CPE1

(capacity of the fractal interface CPE). The impedance of the CPE element is calculated by:

$$Z_{CPE} = \frac{1}{Q(j\omega)^\alpha} \quad (7)$$

where Q and α are frequency-independent parameters, j and ω represent the imaginary unit and the angular frequency, respectively. Q indicates the value of the capacitance of the CPE element, $\alpha=1$ indicates a perfect capacitance, while the lower α value reflects the roughness of the electrode. The real and imaginary parts of the whole impedance of this circuit were calculated according to the following expressions:

$$Z'' = \frac{R_p^2 Q \omega^\alpha \sin(\frac{\alpha\pi}{2})}{(1 + R_p Q \omega^\alpha \cos(\frac{\alpha\pi}{2}))^2 + (R_p Q \omega^\alpha \sin(\frac{\alpha\pi}{2}))^2} \quad (9)$$

368K). Additionally, the low capacitance value (picofarad order) is usually due to grain response rather than to grain boundary of which higher capacitance value is in the nanofarad to the microfarad order [30].

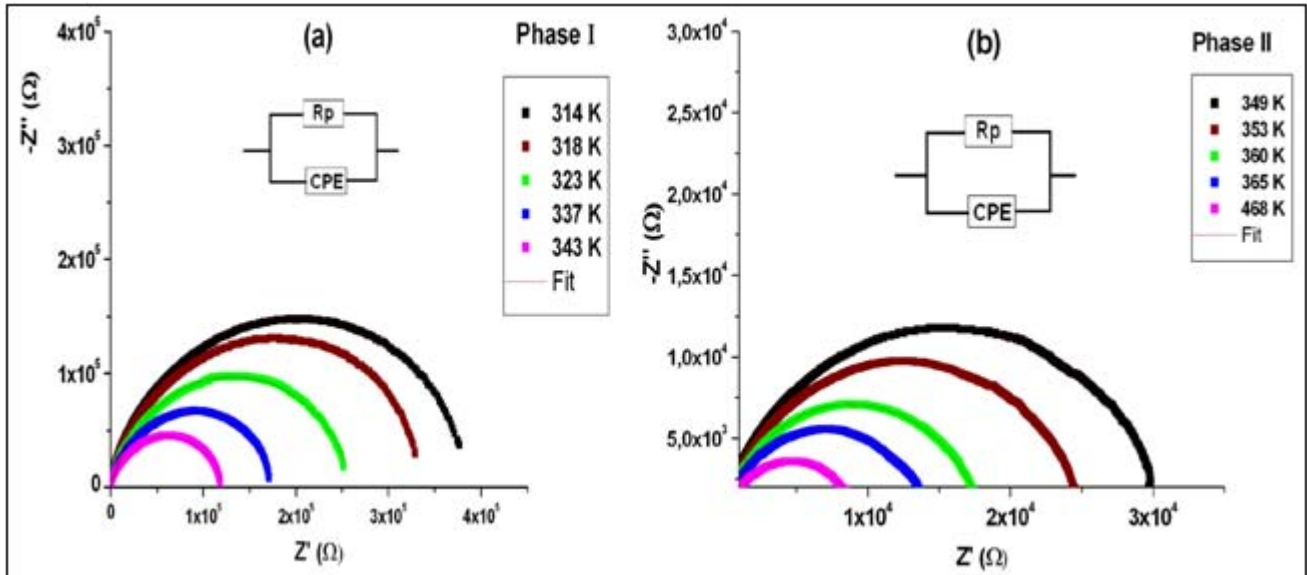


Figure 8: Cole–Cole plots of the $(C_6H_5NH_3)_2SnCl_6$ compound at several temperatures for the both phases I (a) and II (b). The inset figure shows the equivalent circuit model of the $(C_6H_5NH_3)_2SnCl_6$ compound. The solid line is a fit of the experimental data

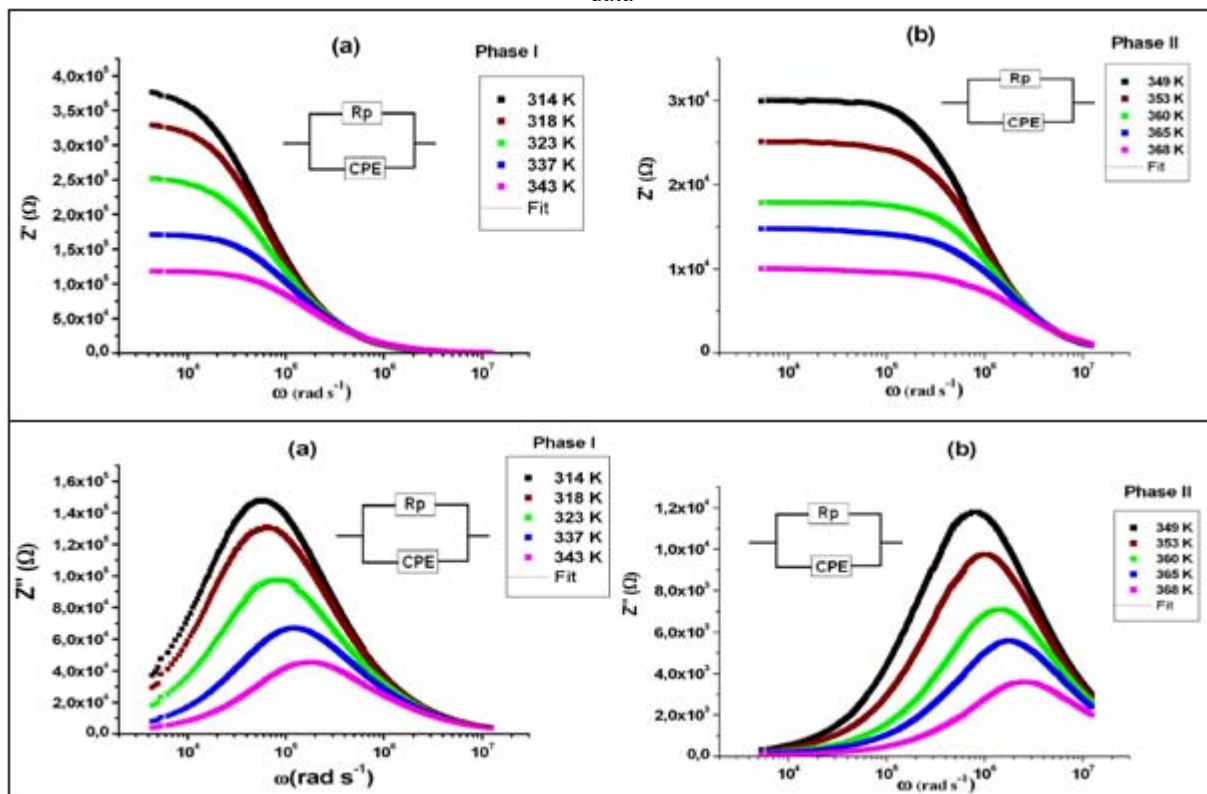


Figure 9: Variation of the real part (a) and the imaginary part (b) of the impedance as a function of angular frequency at several temperatures. The solid line is a fit of the experimental data

5.2. Conductivity Analysis

The magnitude of bulk conductivity, σ_p , can be calculated from the bulk resistance, R_p , by the relation:

$$\sigma_p = \frac{e}{S * R_p} \quad (10)$$

where S is the electrolyte-electrode contact area and e the thickness of the sample. The bulk resistance R_p can be determined at the low-frequency side of the bulk arc ($R_p = \lim|Z|, \omega \rightarrow 0$). The temperature dependence of the σ_p conductivity versus $(1/T)$ is shown in Fig. 10. The

temperature variation of the conductivity plot of $(C_6H_5NH_3)_2SnCl_6$ shows two straight-line regions with a change in the slope around 343K. In both regions, the conductivity follows the Arrhenius relation:

$$\sigma_p \cdot T = \sigma_0 \exp\left[-\frac{E_p}{k_B T}\right] \quad (11)$$

where σ_0 is the pre-exponential factor, E_p denotes the conductivity activation energy and k_B is the Boltzmann constant. The conductivity increases at a higher rate in phase II and at a slower rate in phase I. The activation energies

calculated for both phases I and II are $E_p=0.563$ eV, and $E_p=0.405$ eV, respectively.

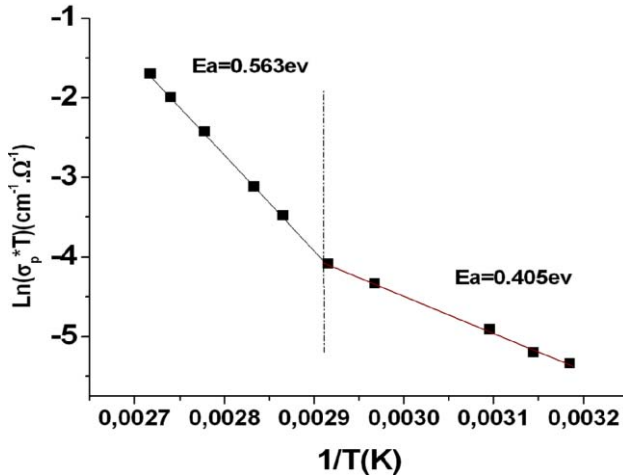


Figure 10: Arrhenius plot of σ_p conductivity in $(C_6H_5NH_3)_2SnCl_6$

5.3. Frequency and temperature dependence of the AC conductivity

The real part of the total conductivity $\sigma'_{Tot}(\omega, T)$ is calculated using the following expression:

$$\sigma'_{Tot}(\omega, T) = \frac{e}{S} \frac{Z'}{(Z'^2 + Z''^2)} \quad (12)$$

where e , S , Z' and Z'' are the thickness, the area of the sample, the real and the imaginary parts of the complex impedance, respectively.

The frequency dependence of the real part of conductivity plots ($\sigma_{Tot} = f(\omega, T)$) at various temperature for $(C_6H_5NH_3)_2SnCl_6$ is depicted in Fig. 11.

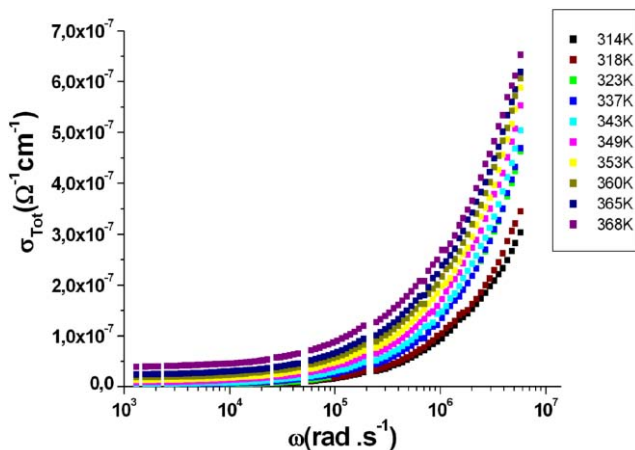


Figure 11: Frequency dependence of the conductivity at various temperatures

The real part of the conductivity clearly reveals a frequency independent part at low frequency end followed by a frequency dependent part at high frequencies, reflecting the conductivity dispersion phenomenon [31] which is usually analyzed using Jonscher's universal power law [32]:

$$\sigma'(\omega, T) = \sigma_{DC}(T) + A(T)\omega^{s(T)} \quad (13)$$

where ω is the angular frequency, $\sigma_{DC}(T)$ is the frequency-independent part of the conductivity, $A(T)$ is a constant for a particular temperature and $s(T)$ is a fractional exponent ranging between 0 and 1. The values of $S(T)$ for an ideal Debye dielectric dipolar-type and ideal ionic-type crystal are 1 and 0, respectively [33]. Fig. 12 shows the variation of the fitted values of the reciprocal $A(T)$ and $s(T)$ with temperature, respectively. Both parameters decrease with temperature. The change of the slope observed around 343 K confirms the phase transition detected by the DSC and $\text{Ln}(\sigma_p \cdot T) = f(1/T)$ measurements. The reciprocal temperature dependence of the $\text{Ln}(\sigma_{DC} \cdot T)$ conductivity is shown in Fig. 13. This plot shows that the DC conductivity exhibits an Arrhenius-type temperature dependence given by the following relation:

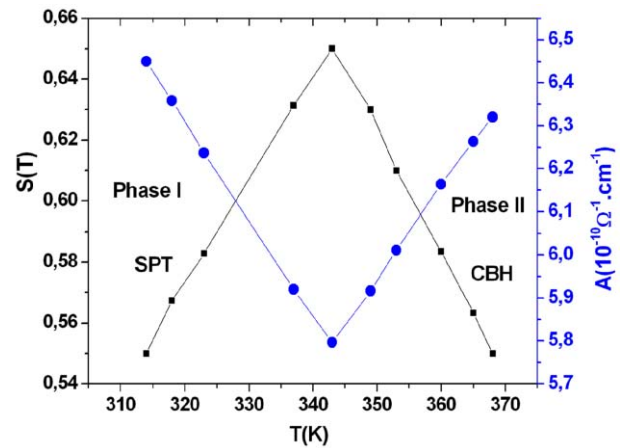


Figure 12: Temperature dependence of the frequency exponent S and the preexponential factor A

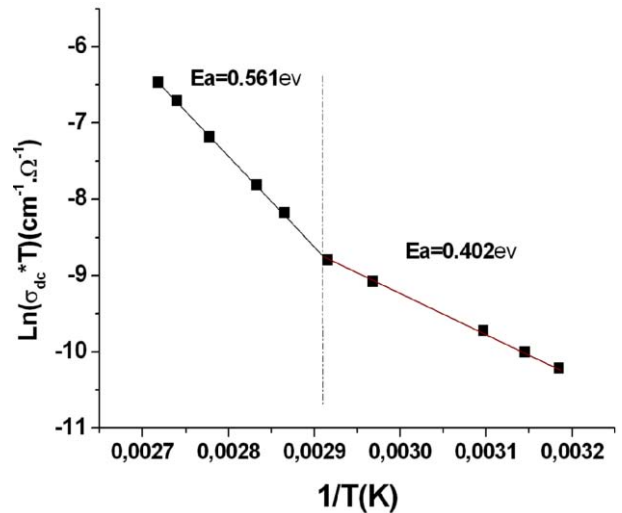


Figure 13: Arrhenius plot of DC conductivity in $(C_6H_5NH_3)_2SnCl_6$. The solid lines represent least-squares fitting

$$\sigma_{DC} = \sigma_0 \exp\left(-\frac{E_{DC}}{k_B T}\right) \quad (14)$$

where σ_0 is the pre-exponential factor, E_{DC} is the activation energy for the DC conduction, and k_B is the Boltzmann constant [34]. The values of the activation energies determined in phases I and II are 0.561 eV and 0.405 eV, respectively. These values are similar to those determined by the σ_p bulk conductivity.

6. Conclusions

The single X-ray diffraction of the $(C_6H_5NH_3)_2SnCl_6$ indicates that this salt belongs to the $P2_1/c$ space group. Phenylammonium cation and hexachlorostannate anion linked via simple $NH...Cl$ hydrogen bond. Infrared and Raman spectra of $(C_6H_5NH_3)_2SnCl_6$ were recorded at 298 K and discussed. The assignment of the observed Raman lines was performed by comparison with the homologous compounds. The AC conductivity of this material has been studied as a function of temperature and frequency. The frequency-dependent conductivity of this material at different temperatures has been analyzed using Jonscher's power law. The close value of activation energies obtained from the analysis of equivalent circuit and conductivity confirms the presence of the hopping mechanism. The conduction mechanism is attributed to the SPT and CBH model.

7. Supplementary Material

CCDC 924479 contains the supplementary crystallographic data for this paper. These data can be obtained free of charge via www.ccdc.cam.ac.uk/conts/retrieving.html (or from the Cambridge Crystallographic Data Centre, 12, Union Road, Cambridge, CB2 1EZ, UK (fax: +44 (1223) 336-033; e-mail: deposit@ccdc.cam.ac.uk).

8. Acknowledgements

- The authors gratefully acknowledge the support of the Tunisian Ministry of Higher Education and Scientific Research and the technical help for the X-ray data collection rendered by A. Ben Salah, Professor at the Faculty of Science of Sfax.
- The authors thank Prof. Kamel Guidara of the Faculty of Sciences of Sfax-Tunisia for assistance with the impedance measurements.

References

- [1] Pamela, J., Douglas, H., Zubieta J; Chem. Int. Ed. **38** (1999) 2638.
- [2] Arno, K., Andrew, G. C., Holmes, A. B., Angew J; Chem. Int. Ed. **37**(1998) 402.
- [3] Calabrese, J., Jones, N. L., Harlow, R. L., Herron, N., Thorn, D. L., Wang Y. J; Chem. Soc. **113**(1991) 2328.
- [4] Sekine, T., Okuno, T., Awaga K; Acta Cryst. **E61**(1998) 577.
- [5] Xu, Z., David, B. M., Dimitrakopoulos, D. D., Maxcy K. R; Inorg. Chem. **42**(2003) 2031.
- [6] Xu, Z., David, B. M; Chem. Mater. **15**(2003) 3632.
- [7] David, B. M., Field, C. A., Schlesinger, Z., Laibowitz, R. B; Solid. State. Chem. **114**(1995) 159.
- [8] Wang, S., David, B. M., Field, C. A., Guloy, A; J 1995 Am. Chem. Soc. **117**() 5297.
- [9] George, M. S; SHELXL-97. Program for the Refinement of Crystal Structures. University of Göttingen Germany (1997).
- [10] Zhi, L., Hongxia, D., Jiandong, F., Wentao, Y., Xutang, T., Minhua, J; Z Kristallogr. **224**(2009) 79.

- [11] Rademeyer, M., Lemmerer, A., Billing, D. G; Acta Crystallogr. **C63**(2007) 101.
- [12] Soufian, B., Merazig, H., Beghidja, A., Beghidja, C; Acta Cryst. **E61**(2005) 577.
- [13] Yatsenko, A. V., Medvedev, S. V., Aslanov, L. A., Yashina, N. S., Petrosyan, V. S; Struct. Chem. **27**(1986) 324.
- [14] Karoui, S., Kamoun, S., Michaud, F; Acta Cryst. **E69**(2013) m187.
- [15] Ertl, A., Hughes, J.M., Pertlik, F., Foit, F.F., Wright, S.E., Brandstätter, B., Marler, F; Can. Mineral. **40**(2002) 153.
- [16] Boultif, A., Louer, D ; J. Appl. Crystallgr. **37**(2004) 724.
- [17] Edgar, W. B., Decius, J. C., Cross, P. C; McGraw, H. N.Y; (republished by Dover: New York, 1980) (1955).
- [18] Annama, J., Daizy, P., Abdullah, K. I., Gabor, K., Devanarayanan, S; Raman Spectrosc. **31**(2000) 1067.
- [19] Roeges, N. P. G; Wiley, Chichester (1994).
- [20] Young, C. W., Duvall, R., Wright, B; Anal. Chem. **23**(1951) 709.
- [21] Bomstein, J ; Anal. Chem. **25**(1953) 512.
- [22] McMuney, H. L., Vernon T; Anal. Chem. **24**(1952) 318.
- [23] McCaulay, D. A., Lien, A. P., Launer, P.J; J. Am. Chem. Soc. **76**(1954) 2354.
- [24] Canon, C. G., Sutherland, G. B. B. M; Spectrochim. Acta. **4**(1951) 373.
- [25] Plyler, E. K; Discussion of the Faraday Soc. **9**(1950) 100.
- [26] Pitzer, K. S., Scott D.W; J. Am. Chem. Soc. **65**(1943) 803.
- [27] Jeghnou, H., Ouasri, A., Rhandour, A., Dhamelincourt, C., Dhamelincourt, P., Mazzah A; J. Raman Spectrosc. **34**(2003) 399.
- [28] Ben Rhaïem, A., Guidara, K., Gargouri, M., Daoud A; J. Alloys Compd. **392**(2005) 87.
- [29] Hajlaoui, S., Chaabane, I., Oueslati, A., Guidara K; Solid State Sci. **25**(2013)134.
- [30] Haittao, Ye., Sun, C., Hung, D., Hing, P; Thin Solid Films. 381(2001).
- [31] Jonscher, A. K; Nature. **267**(1977) 673.
- [32] Ben Rhaïem, A., Guidara, K., Gargouri, M., Daoud, A; J. Alloys Compd. **392**(2005) 87.
- [33] Nadeem, M., Akhtar, M. J., Khan A. Y; Sol. State Commun. **134**(2005) 431.
- [34] Muralidharan, P., Venkateswarlu, M., Satyanarayana, N; J. Non-Cryst. Solid. 351(2005).